2

Application of Monte Carlo Simulation in Optical Tweezers

Yu-Xuan Ren[1], Jian-Guang Wu[2] and Yin-Mei Li[3]
[1,2,3]*University of Science and Technology of China, Hefei, 230026*
[2]*AnHui University of Technology, Maanshan, 243032*
People's Republic of China

1. Introduction

The concept of optical tweezers(Ashkin et al., 1986) was first conceited by Ashkin et al in 1986. From then on, optical tweezers expands broad research application areas, such as colloidal sciences(Pesce et al., 2009), biophysics(Abbondanzieri et al., 2005; Zhang et al., 2006) and statistical mechanics(Li et al., 2010; McCann et al., 1999). Generally, the probe in optical tweezers' experiment is micrometer-sized or nano- bead, e.g. polystyrene bead, which can be stick to glass surface or chemically linked to biological macromolecules to further reveal the mechanical properties of molecules such as protein or DNA. The trapped bead in optical tweezers is not stationary like mechanical tweezers; it may suffer from random work with its displacement signal obeying Brownian statistics. Analysis of the Brownian motion signal of the trapped probe generates numerous information of the macromolecules, e.g. force, step motion. Therefore, the motion of probe is of great importance in these experiments. Monte Carlo technique provides simulation tools in these experiments to theoretically study the motion of beads in optical tweezers to further reveal the new phenomenon that governs the nature of trapped beads, the characteristics of the optical trap itself and even the mechanical property of macromolecules chemically linked with the trapped microsphere.

The optically trapped microsphere encounters numerous collisions from the surrounding molecules, which constitutes the origin of random forces. The trapped bead behaves like a drunker doing random walk. The topic of analyzing the motion equation of the trapped bead is in the scope of Monte Carlo simulation. In this chapter, we start with the description of light induced radiation force and review the hydrodynamic equation that describes the Brownian motion of trapped bead in optical tweezers in the second and third part, followed by adoption of Monte Carlo simulation in this specific case. In the fourth and fifth parts of this chapter, we show the application methods by presenting two examples of time-sharing optical tweezers and oscillatory optical tweezers in sequence. The sixth part of this chapter discusses potential applications of Monte Carlo simulation in practical colloidal sciences such as artificially induced collision by optical tweezers. This chapter is summarized in the last part.

2. Principle of optical tweezers

In macroscopic world, one may use a mechanical tweezers to manipulate an object firmly. What about microscopic manipulation? Optical micromanipulation provides a non-contact,

low destructive and gentle means to manipulate microscopic objects. Ashkin et al had proved that tightly focused laser beam is able to confine microsphere, such as cell, flagellar, colloids etc, due to radiation pressure of light. This concept was then developed to a widely used tool, optical tweezers. The detailed analysis of optical tweezers may be found in many early original literatures and recent review articles. We here briefly review two commonly used methods explaining the forces of a particle in optical tweezers according to the relative geometrical dimension of the particle to that of the wavelength.

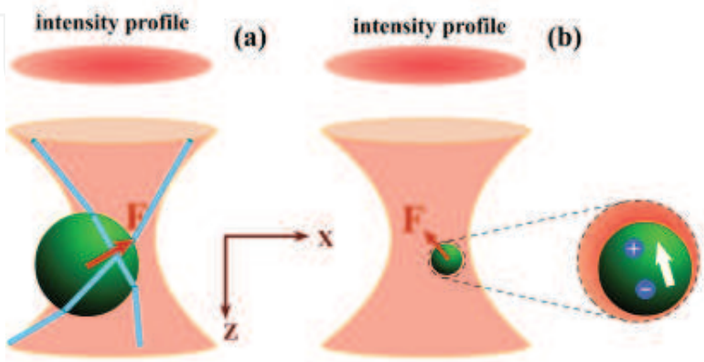

Fig. 1. Principle of optical tweezers. (a) Ray tracing approach based on geometrical optics, (b) multiple dipole model with electromagnetics.

The first approach illustrating the principle of optical tweezers is based on ray optics when the dimension of the particle is greater than the working wavelength as is shown in Fig.1(a). In ray tracing methods, a single optic ray with a portion of power P is considered hitting the dielectric sphere with incident angle θ and incident momentum per second $n_1 P/c$. The resultant force on the sphere is the sum of contributions due to the reflected ray of power PR and the infinite number of emergent refracted rays of successively decreasing power PT^2, PT^2R,...PT^2R^n,....The quantities R and T are the Fresnel reflection and transmission coefficients of the surface at θ. The net force from the origin can be decomposed into F_z and F_x components as follows(Ashkin, 1992)

$$F_z = F_{scat} = \frac{n_1 P}{c}\{1 + Rcos(2\theta) - \frac{T^2[cos(2\theta - 2\gamma) + Rcos(2\theta)]}{1 + R^2 + 2Rcos(2\gamma)}\} \tag{1}$$

$$F_x = F_{grad} = \frac{n_1 P}{c}\{Rsin(2\theta) - \frac{T^2[sin(2\theta - 2\gamma) + Rsin(2\theta)]}{1 + R^2 + 2Rcos(2\gamma)}\} \tag{2}$$

The total scattering and gradient forces are the sum of the above single ray scattering and gradient forces over all probable incident rays.

For those particles with diameter much less than the working wavelength of laser beam, the scattering force and gradient force are calculated electromagnetically. The dielectric sphere is induced by strongly focused light with multiple dipole, and the resultant force is considered as the interaction between light field and the induced multiple dipole. Followed by (Ashkin et al., 1986), the scattering force is related to the incident power through $F_{scat} = n_p P_{scat}/c$, where P_{scat} is the scattered power. In terms of the intensity I_0 and the effective refractive index m

$$F_{scat} = \frac{I_0}{c}\frac{128\pi^5 a^6}{3\lambda^4}(\frac{m^2 - 1}{m^2 + 2})^2 n_p \tag{3}$$

The gradient force F_{grad} along the direction of the intensity gradient for a Rayleigh spherical particle with polarizability α is

$$\mathbf{F}_{grad} = -\frac{n_p}{2}\alpha\nabla E^2 = -\frac{n_p^3 a^3}{2}\frac{m^2-1}{m^2+2}\nabla E^2 \tag{4}$$

Both approaches are able to estimate the trapping ability. We here take electromagnetic model as an example to estimate the trapping behavior. Consider the laser intensity can be rewritten via the time-averaged Poynting vector(Ou-Yang, 1999)

$$I = \langle S\rangle = \frac{1}{2}\frac{1}{\mu_1 n_1 c}|E|^2 = \frac{c\epsilon_0 n_1}{2}|E|^2 \tag{5}$$

The intensity distribution relies on the type of trapping beam used. Many intensity profiles can be used in optical trapping experiments, such as Laguerre-Gaussian beam(Ren, Li, Huang, Wu, Gao, Wang & Li, 2010; Ren, Wu, Zhou, Fu, Sun, Wang & Li, 2010), radially polarized beam(Kozawa & Sato, 2010), etc. Here we consider the most commonly utilized single beam optical trap with Gaussian intensity profile

$$I = I_0 e^{-\frac{r^2}{\omega^2}} \tag{6}$$

where ω is the $1/e$ width of Gaussian intensity profile along the radial direction. Inserting Eqs. 5 and 6 into Eq. 4 yields

$$\mathbf{F}_{grad} = \frac{2n_p^3 a^3}{c\epsilon_0 n}\frac{m^2-1}{m^2+2}\mathbf{r}e^{-\frac{r^2}{\omega^2}} \equiv k_r \cdot \mathbf{r}e^{-\frac{r^2}{\omega^2}} \tag{7}$$

The gradient force approximately satisfies Hooke's law for significantly small displacements with spring constant k_r. The spring constant characterizes how stiff the optical trap is, and it has an alternative name, trap stiffness. Experimentally the trap stiffness can be determined by equipartition theorem $\frac{1}{2}k_B T = \frac{1}{2}k\langle x^2\rangle$ through measurement of Brownian motion positions, where x stands for the position of trapped microsphere.

3. Dynamics of optically trapped beads

From the microsphere's point of view, it encouters random forces, optical restoring force, frictional force and inertia force. This provides a new approach to evaluate the trap stiffness both experimentally and simulatively. Practically, it is a good approximation utilizing the parabolic potential well model to describe the single beam optical trap. Since the microsphere in the aqueous solution encounters numerous collisions by liquid molecules from all around randomly, the microsphere moves accordingly and the one-dimensional motion equation is characterized by the following Langevin equation

$$m\ddot{x} + \gamma\dot{x} + kx = \sqrt{2k_B T\gamma}\xi(t) \tag{8}$$

where k is the static stiffness of an optical trap, m denotes the mass of the microsphere, $x(t)$ represents the instantaneous position of the microsphere at time t, $k_B T$ is thermal energy, $\gamma = 6\pi\eta a$ with γ being the viscosity coefficient of surrounding medium, and $\xi(t)$ depicts a random Gaussian process satisfying

$$\langle\xi(t)\rangle = 0 \tag{9}$$

$$\langle \xi(t)\xi(t') \rangle = \delta(t - t') \tag{10}$$

In low Reynolds number case, the trapped microsphere is well approxiated to an overdamping vibrator, therefore the inertia term is much smaller than the viscous drag force term and can be ignored. The simplified Langevin equation is

$$\gamma \dot{x} + kx = \sqrt{2k_B T \gamma}\xi(t) \tag{11}$$

Monte Carlo simulation is employed to model the random Gaussian process $\xi(t) = \sqrt{-2ln(u)}cos(2\pi v)$, where u and v are two uniformly distributed random numbers ranging in $(0, 1)$. The simulation algorithm can be deduced from Eq. 8 as follows

$$x_n = x_{n-1} + v_{n-1}\tau \tag{12}$$

$$v_n = v_{n-1} - \frac{kx_{n-1}\tau}{m} + \frac{\sqrt{12\pi k_B T \eta a \tau}}{m} \times \sqrt{-2ln(u)}cos(2\pi v) - v_{n-1}\frac{6\pi\eta a}{m}\tau \tag{13}$$

where τ indicates the length of the time grid, x_n is the n^{th} elementary position, namely the position at the n^{th} time grid, v_n is the instantaneous velocity of the microsphere correspondingly. Careful attention must be taken to select proper time step to describe the motion of microsphere, since large time step may poorly describe the random process while smaller time step induces longer computation time.

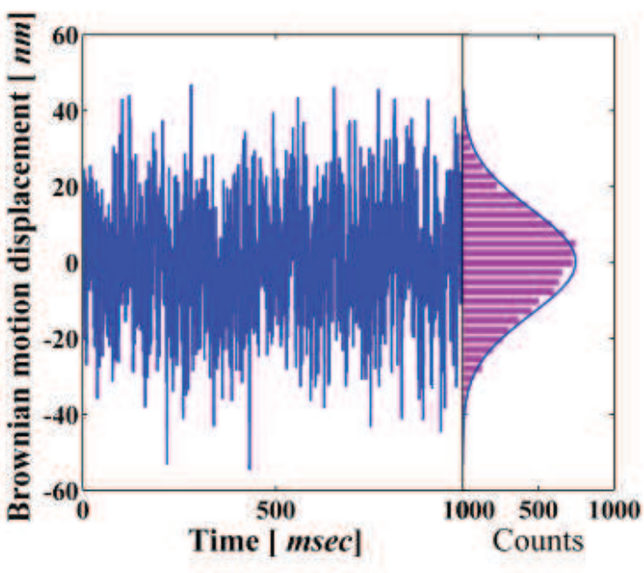

Fig. 2. Brownian motion signal and its histogram. The trapped bead is $3\mu m$ diameter polystyrene microsphere and the initial optical trap stiffness $20pN/\mu m$ in the simulation. The histogram indicates the standard deviation is $\sigma = 13.86nm$.

Note that the trap stiffness k may be numerically calculated *ab initio* through ray optics model or electromagnetic model regarding different sizes of spheres without consideration of optical transmittances and losses of instruments. It is very difficult to predict accurately the actual stiffness if the shape of microsphere is different from each other. Experimentally, due to limited detection speed and systematic noises, the actual stiffness can not be accurately determined either. We here postulate an ideal k value(true stiffness) throughout Monte Carlo simulation.

The resultant stiffness(measured stiffness) are evaluated through commonly used methods, such as power spectra, equipartition theorem.

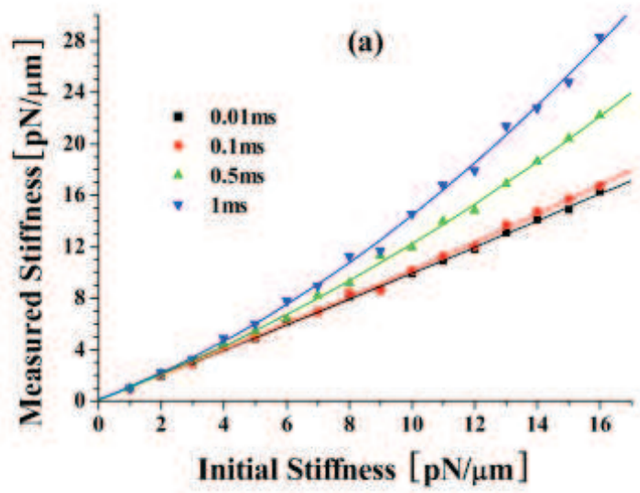

Fig. 3. Measured stiffness varies with respect to initial stiffness under different exposure time performed with Monte Carlo simulation by Gong et al when the trapped bead is $1\mu m$ diameter polystyrene bead(Gong et al., 2006).

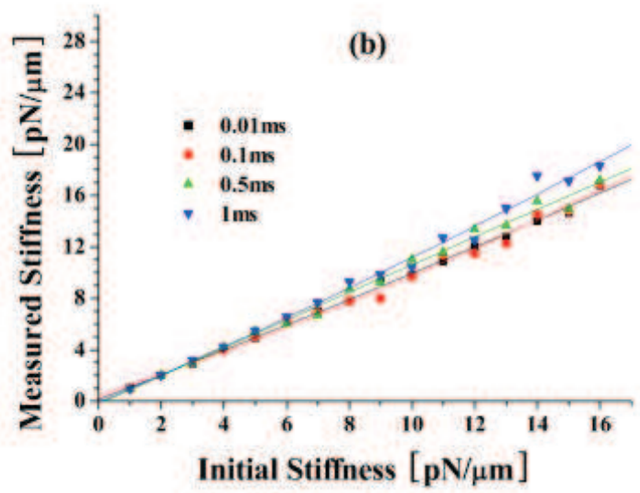

Fig. 4. Measured stiffness varies with respect to initial stiffness under different exposure time performed with Monte Carlo simulation by Gong et al when the trapped bead is $3\mu m$ diameter polystyrene bead(Gong et al., 2006).

Throughout this chapter, the time step is taken as $10ns$. We checked the performance of the algorithm with the following parameters: the initial position of the microsphere is in the trap center with displacement and velocity values all 0. The temperature is $300K$ with the coefficient of viscosity $0.801 \times 10^{-3} kg/(m \cdot s)$. The trapped bead is $3\mu m$ diameter polystyrene

microsphere with initial optical trap stiffness $20pN/\mu m$. The simulated trajectories describing the stochastic motion process of the bead is illustrated in left part of Fig.2. The right hand side of Fig.2 indicates the histogram with its standard deviation $\sigma = 13.86nm$. Accordingly, one can calculate the measured stiffness by Monte Carlo simulation through equipartition theorem with the result that $k_{mea} = k_B T/\langle\sigma^2\rangle = 21.7pN/\mu m$, which is greater than the initial stiffness $20pN/\mu m$. This indicates that the measured stiffness deviates upwards to the initial stiffness or exact stiffness and is of great significance for actual experiments to select proper experimental parameters, such as exposure time of detector. To further reveal the relationship between the measured stiffness and initial stiffness, Gong et al performed a series of Monte Carlo simulations with different integration times(Gong et al., 2006). Fig.3 shows this relation for $1\mu m$ diameter polystyrene microsphere with integration time $0.01ms$, $0.1ms$, $0.5ms$ and $1ms$ correspondingly denoted by square, circle, upward triangle and downward triangle. The total data collection time in the simulation adopts $5s$. We conclude that the higher the acquisition time of the measurement is for a trapping system, the more the measured stiffness values deviate upwards from the initial values.

Another series of simulation were performed for $3\mu m$ diameter polystyrene spheres with similar conclusions as is illustrated in Fig.4. Two conclusions can be made according to comparision between Figs. 3 and 4. First, for those beads with greater geometrical parameters, the measured stiffness deviates smaller than those with smaller spatial dimension with the same initial stiffness and exposure time. Second, the measured stiffness for less stiffer trap deviates upwards smaller than that for more stiffer trap for polystyrene beads with different sizes. The significance of these findings is that in biophysical experiments, researchers may select significantly larger beads as probe instead of smaller ones when the integration time is not small enough. Alternatively, significantly smaller integration time is employed when the probe adopts smaller nanometer-sized beads, but it cannot be infinitely small due to the limitation of the data acquisition speed of modern detectors.

In order to verify the dependence of measured stiffness with respect to initial stiffness, Gong et al analysed the relation with power spectrum as comparison(Gong et al., 2006). Results from both methods agree well with each ether. This reflects that our algorithm performs well and can be used for further research.

4. Effecitive stiffness of time-sharing optical tweezers

Time-sharing optical tweezers (TSOT) (Liao et al., 2008; Wu et al., 2009) is a very effective technique that produces multiple optical tweezers by splitting a single laser beam at different time intervals to stretch bio-macromolecules or the membrane of human red blood cells. Experimental physicists use various kinds of instruments, such as acousto-optic deflector(AOD)(Emiliani et al., 2004)or a piezoelectric scanning mirror(Mio et al., 2000; Sasaki et al., 1991) to translate light slightly at different frequencies to fulfill quasi-stationary multiple optical traps(Dame et al., 2006).Some novel and practical means are also employed to perform the same function, and a typical example is the rotating glass based time-sharing technique(Ren, Wu, Chen, Li & Li, 2010). Though the above methods employed are different from each other, the realized quasi-stationary traps are all TSOT. In TSOT, The laser beam serves a certain trap at a time interval and immediately switches to another spatial location to serve a new one as is illustrated in Fig.5. For a specific location, the laser switches on and off periodically. Sequential diagram of a trap formed through time-sharing technique is also shown in Fig. 5. The ratios of durations with laser on and off is defined as duty ratio of a TSOT with the following form

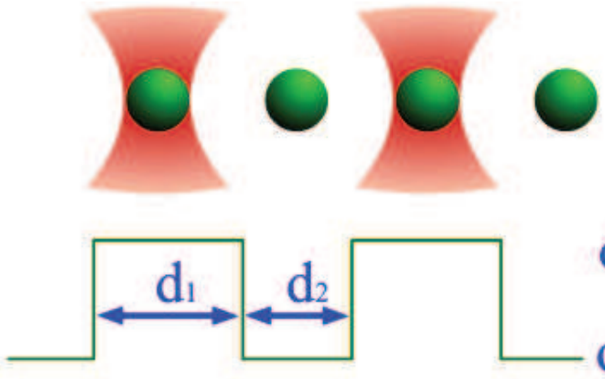

Fig. 5. Schematic diagram of TSOT and its sequential diagram. d_1 and d_2 represent the duration of laser on and off respectively. The periodicity is $T = d_1 + d_2$.

$$D = \frac{d_1}{d_2} \tag{14}$$

where d_1 and d_2 represent durations with laser on and laser off respectively in one period, and the sum of them is trap switching periodicity $T = d_1 + d_2$. Accordingly, the trap switching frequency f_{sw} can be written as follows

$$f_{sw} = \frac{1}{d_1 + d_2} \tag{15}$$

Generally, the Brownian motion of a microsphere in aqueous solution is classified into two categories. The first one is that the bead does confined Brownian motion with trapping laser on, while the second is that the bead does free Brownian motion without the exposure of trapping laser. In confined Brownian motion, the trapped bead not only encounters the viscous drag force and stochastic force, but also suffers from restoring force from strongly focused laser beam. The free Brownian motion means that the laser beam does not act on the bead. When the laser switches on one of the multiple trapping positions, the confined Brownian motion of a trapped bead is simulated using Monte Carlo technique. Because the fast beam deflection is very well achieved by the use of AOD or high speed scanning mirror and the rise time to produce different trap positions is of the order of μs, which is smaller than the trap switching periodicity of several orders, the rise time is neglected in our simulation model as a proper assumption.

Due to the limited bandwidth of recent detectors, it is a great challenge to investigate the effective stiffness of TSOT under a broad range of frequency domain. Theoretically, for the motion of microsphere trapped in TSOT, the solution to the Langevin equation can be analytically found by Fourier analysis with a large number of differential equations. Both experiment and theory find it difficult to reveal the variation of effective stiffness with respect to trap switching frequency. Quantitatively, the use of fast beam deflectors is of crucial importance as the time the trap is 'off', servicing another position, has to be much shorter than the time the particle needs to diffuse away from its trapping position(Emiliani et al., 2004). The more time the trap is 'on', the stiffer the trap is. To better understand the stability property of time-sharing multiple optical traps, we use Monte Carlo technique to simulate the motion of a bead in a time-sharing optical trap in a large frequency domain, and numerically calculate the

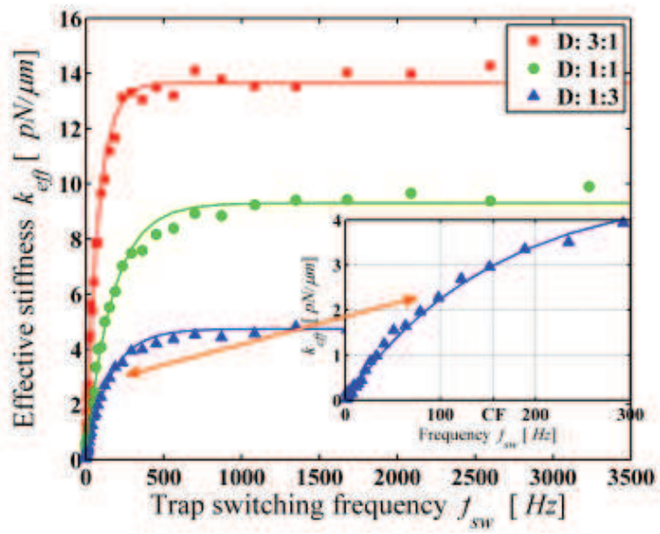

Fig. 6. Effective stiffness varies with respect to trap switching frequency in a long frequency domain for a $2\mu m$ diameter polystyrene bead performed by Monte Carlo simulation under TSOT with different duty ratio(Ren, Wu, Zhong & Li, 2010).

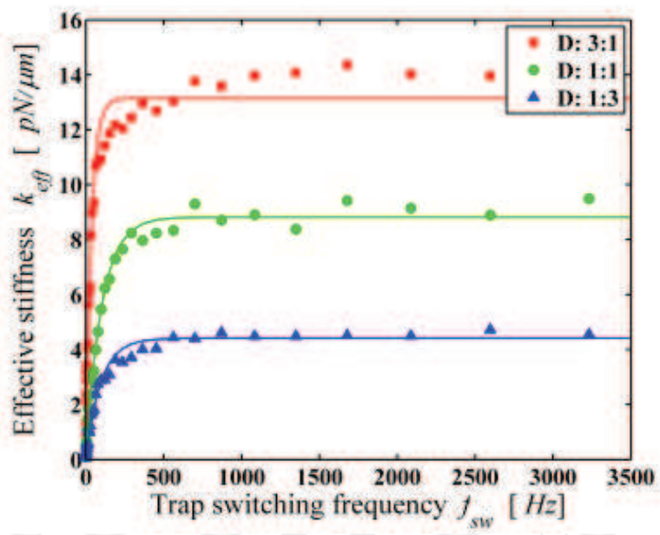

Fig. 7. Effective stiffness varies with respect to trap switching frequency in a long frequency domain for a $3\mu m$ diameter polystyrene bead performed by Monte Carlo simulation under TSOT with different duty ratio(Ren, Wu, Zhong & Li, 2010).

effective stiffness of time-sharing optical tweezers according to equipartition theorem. Further the relationship between effective stiffness and trap switching frequency can be revealed. Throughout the simulation, the temperature is set at 298 Kelvin, with drag coefficient of aqueous solution $0.894 \times 10^{-3} kg/(m \cdot s)$. The microsphere adopts polystyrene bead with mass density being $1.05 \times 10^{-3} kg/m^3$. Initially, the simulated bead is at the equilibrium position with velocity zero. When the laser is switched on, the stiffness k in Eq. (3) is equal to $18pN/\mu m$, and while the laser off, k is set to zero during simulation. For continuous wave laser tweezers,

the stability property of a trap is characterized by a stiffness adopting equipartition theory. Similarly, effective stiffness is defined to characterize time-sharing optical tweezers, and it reads

$$k_{eff} = \frac{k_B T}{\sigma^2} \tag{16}$$

In the simulation, the effective stiffness is numerically calculated from 10000 measurements of Brownian motion positions. The simulation shows that for $2\mu m$-diameter polystyrene bead diffused in aqueous solution, the effective stiffness increases with trap switching frequency under different duty ratios as is shown in Fig. 6. The effective stiffness of TSOT with duty ratio $3:1$ increases sharply with trap switching frequency when the frequency is smaller than $500Hz$; while the frequency is larger than $500Hz$, the effective stiffness does not vary with respect to trap switching frequency. This general relation holds for other duty ratios, e.g. $D = 1:1$ and $D = 1:3$. The relation is linear when the frequency domain is significantly small for TSOT with duty ratio $1:3$ as illustrated in inset of Fig. 6. In low frequency range, this relation is linear and is verified experimentally by Ren et al through glass plate based TSOT in the frequency range from $5Hz$ to $70Hz$(Ren, Wu, Chen, Li & Li, 2010). Similar results for $3\mu m$-diameter polystyrene bead are shown in Fig. 7 from Monte Carlo simulation. The results for beads with diameter of both $2\mu m$ and $3\mu m$ indicate a general trend for the relationship between effective stiffness and switching frequency.

To analytically describe the dependence of stiffness on the trap switching frequency, we employ Box Lucas Model(Box & Lucas, 1959), which was first introduced to describe the quantum yield of intermediate product of a consecutive chemical reaction, to fit our simulation dependence of effective stiffness on trap switching frequency. The analytical relation is qualitatively described by $k_{eff} = k_0 \cdot (1 - exp(-f_{sw}/f_{ch}))$, where k_0 and f_{ch} stand for transient-free stiffness and characteristic frequency respectively. For $2\mu m$ diameter polystyrene bead trapped in TSOT with duty ratio $1:3$, the fitted values of the two parameters are: $k_0 = (4.74 \pm 0.05)(pN/\mu m)$ and $f_{ch} = (156 \pm 6)(Hz)$ with coefficient of determination R^2 being 0.9839 which means the Box Lucas Model well describes the dependence of effective stiffness on switching frequency in a large frequency domain. In inset of Fig.6 there are two letters CF marked on the horizontal axis, and this mark indicates where characteristic frequency locates for $2\mu m$-diameter bead trapped in TSOT with duty ratio $1:3$. Following the same procedure, the parameters k_0 and f_{ch} for beads with different diameters in TSOT with different duty ratios are summarized in Table 1.

Table 1. Summation of k_0 and f_{ch} of time-sharing optical tweezers with different duty ratios(Ren, Wu, Zhong & Li, 2010).

Duty ratio	$2\mu m$		$3\mu m$	
	$k_0\ (pN/\ \mu m)$	$f_{ch}\ (Hz)$	$k_0\ (pN/\ \mu m)$	$f_{ch}\ (Hz)$
3 : 1	13.65 ± 0.12	78 ± 3	13.14 ± 0.19	36 ± 2
1 : 1	9.30 ± 0.10	169 ± 7	8.82 ± 0.09	102 ± 4
1 : 3	4.74 ± 0.05	156 ± 6	4.41 ± 0.06	95 ± 5

Actually, in higher frequency ranges, such as the case of femtosecond laser optical tweezers(Zhou et al., 2008), the effective stiffness doesn't vary with the increase of modulation frequency. The trap is stable subjected to change of repetition rate of femtosecond laser with a fixed output power, and the effective stiffness is only affected by the average output power of laser with high repetition rate.

In lower frequency range, the model can be approximated by a linear regression model at high accuracy. When the switching frequency is smaller than the characteristic frequency, namely $f_{sw} < f_{ch}$, simulation results verify that it performs well even using linear regression model, which is of great importance when using unstable TSOT with low switching frequencies such as the case of studying the colloidal collision frequency.
The simulation results indicate that for a certain bead trapped in TSOT with different duty ratios the transient-free stiffness k_0 increases with duty ratio which determines the average power of a certain trap. As for the same bead, the characteristic frequency varies with the duty ratio, and according to our simulation, the characteristic frequency with duty ratio 3:1 is smaller than those with other two duty ratios both for beads with diameter $2\mu m$ and $3\mu m$. A proper explanation is that the effective stiffness transits to a stable value quicker than that with small duty ratio when increasing the trap switching frequency. Meanwhile, the characteristic frequencies with duty ratios 1:1 and 1:3 are larger and close to each other.

5. Dynamics of microsphere under oscillatory optical tweezers

Oscillatory optical tweezers is another derivative of spatially and temporally modulated optical trap. Oscillatory optical tweezers plays its unique role in microrhoelogy and biophysics. It can be used to measure the elastic storage modulus and viscous loss modulus of a material, elasticity of DNA or red blood cell, etc. Oscillatory optical tweezers can be constituted by moving the center of a single beam optical trap sinusoidally with a fixed frequency ω as is shown in Fig.8.

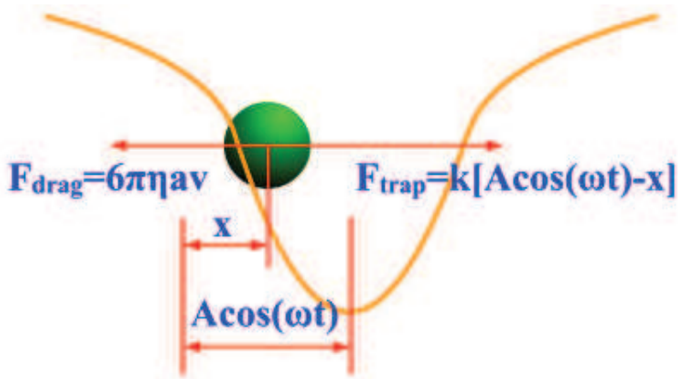

Fig. 8. Schematic diagram representing oscillatory optical tweezers.

Therefore substituting kx in Eq.8 by $k[x - Acos(\omega t)]$ yields the Langevin equation in oscillatory optical tweezers case, and it reads

$$m\ddot{x} + \gamma\dot{x} + k[x - Acos(\omega t)] = \sqrt{2k_B T\gamma}\xi(t) \tag{17}$$

where A stands for the amplitude of oscillation of trap center, ω is the oscillation frequency. The stiffness of a single beam optical tweezers k is not a constant value when the displacement is large enough from the trap center as is shown in Eq.7 and varies nonlinearly with displacement when the position is far away from the center. In this work, we assume the colloidal particle is trapped in the linear region of optical tweezers with k being constant value and the amplitude A is much smaller than the radius of linear region. Similar to the algorithms described in Eq. 12 and 13, the Monte Carlo simulation algorithms can be written as following in the oscillatory optical tweezers' case

$$x_n = x_{n-1} + v_{n-1}\tau \tag{18}$$

$$v_n = v_{n-1} - \frac{k[x_{n-1} - Acos(\omega n\tau)]\tau}{m} + \frac{\sqrt{12\pi k_B T\eta a\tau}}{m} \times \sqrt{-2ln(u)}cos(2\pi v) - v_{n-1}\frac{6\pi\eta a}{m}\tau \tag{19}$$

In the simulation, amplitude A, time step τ, radius of polystyrene bead adopt $50nm$, $1ns$, $100nm$ correspondingly. The coefficient of viscosity is $0.80 \times 10^{-3} kg/(m \cdot s)$ at the temperature of $303K$. The trap stiffness adopts $8pN/\mu m$. Monte Carlo simulation procedures are performed with different oscillation frequencies to generate sequential displacements of trapped sphere.

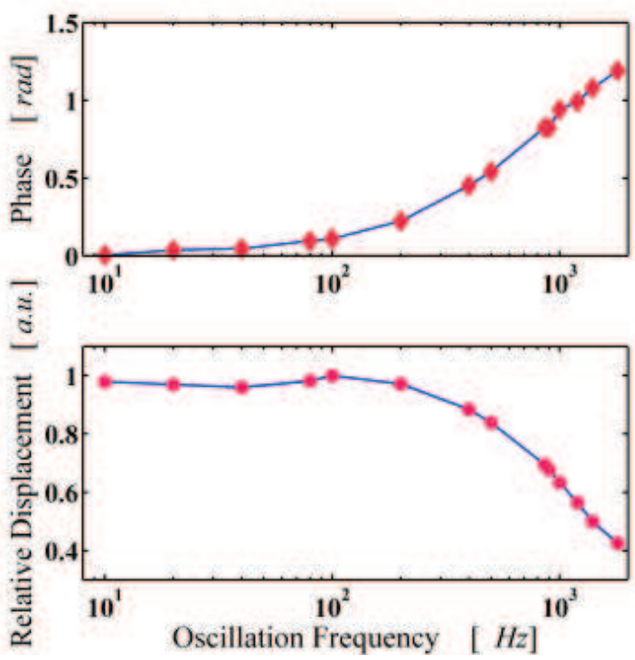

Fig. 9. Phase and displacement of colloidal particles vary with frequencies in oscillatory optical tweezers.

In the simulation, the dynamics of colloidal particle are studied from the output states, which were deduced from the simulated input states(Seol et al., 2004) of colloidal particle encountering in oscillatory optical tweezers. The input states are simulated utilizing the differential form of Eqs. 18 and 19 similar to the procedure of time-sharing optical tweezers(Ren, Wu, Zhong & Li, 2010) or jumping optical tweezers(Liao et al., 2008). Digital lock-in amplifier is adopted to further analyze the simulated displacement signals. The relationship between the movement of the bead and the oscillation of the trap center can be clearly seen by this procedure as is shown in Fig.9. The phase retardation increases with frequency while the amplitude deceases with frequency.

Additionally, when there exists external sources of noise contributing to the motion of the particle, power spectrum analysis was chosen to clearly see the external noise(Horst & Forde, 2008), such as the oscillation of the trap center in oscillation optical tweezers case. In order to analyze the influence of oscillation of the trap center, power spectrum of Brownian positions of colloidal particle with diameter 200nm in oscillatory optical tweezers is analyzed as illustrated in Fig. 10. The curves demonstrated in Fig. 10 show that there exists a resonant peak

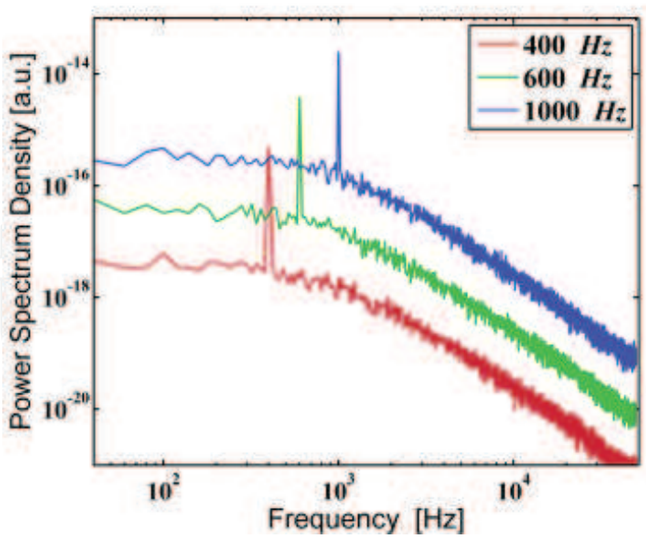

Fig. 10. Power spectrum of colloidal particles trapped in oscillatory optical tweezers with different oscillation frequencies.

typically around $400Hz$, $600Hz$ and $1000Hz$ correspondingly. These resonant frequencies are in accordance with the oscillation frequencies adopted in the simulation. In our simulation, the corner frequency is $f_c = k/(2\pi\gamma) = k/(12\pi^2\eta a) = 8/(12\pi^2 \times 0.8 \times 10^{-3} \times 0.1 \times 10^{-6})Hz = 844Hz$ in the system. The observed peak may be explained by resonance of the particle system to external oscillation.

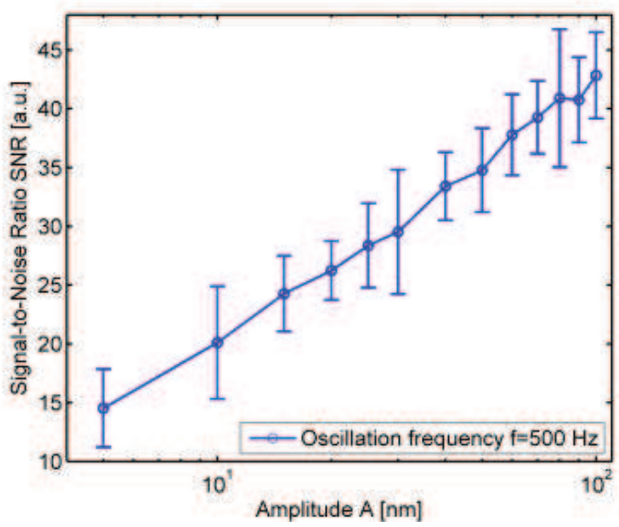

Fig. 11. Signal noise ratio as a function of amplitude of oscillation.

In order to qualitatively investigate the intensity of resonant peak with respect to the oscillation amplitude of the trap center, the signal-noise ratio SNR was introduced to characterize the resonance,

$$SNR = 10log\frac{S(\omega)}{S'(\omega)} \tag{20}$$

where $S'(\omega)$ represents the power spectrum value at the resonant frequency ω without oscillation of the trap center and is evaluated from the power spectrum values around resonance peak, and $S(\omega)$ represents the power spectrum of colloidal particle trapped in oscillatory optical tweezers at frequency ω. Another series of simulations were performed with oscillation frequency $500Hz$ and the microsphere adopts $200nm$ diameter polystyrene bead.

Simulation results demonstrate that the SNR is proportional to the logarithm of oscillation amplitude A of the trap center. This is of great significance to excite oscillation with proper SNR by varying the oscillation amplitude and will have potential applications in measurement of trap stiffness, drag coefficient, particle size and even temperature of the surrounding medium because the resonance intensity is closely related with these parameters.

6. Conclusions

This chapter presents primary examples using Monte Carlo technique in optical tweezers related research and applications. Since optical tweezers has broad applications in colloidal sciences, biophysics, nanotechnology etc., Monte Carlo simulation will find its applications in these interdisciplinary researches. At list 4 topics can be studied indeep, (1) translational diffusion behaviors of colloids under different solvent conditions; (2) rotational diffusion properties induced by strongly focused light with orbital angular momentum; (3) rotational Brownian motion under optical torque for birefringence of innate rotating cell such as motor flagellar; (4) collision of microspheres induced by optical tweezers revealing the stability of colloids.

7. References

Abbondanzieri, E. A., Greenleaf, W. J., Shaevitz, J. W., Landick, R. & Block, S. M. (2005). Direct observation of base-pair stepping by RNA polymerase, *Nature* 438(7067): 460–465.

Ashkin, A. (1992). Forces of a single-beam gradient laser trap on a dielectric sphere in the ray optics regime, *Biophys. J.* 61: 569–582.

Ashkin, A., Dziedzic, J. M., Bjorkholm, J. E. & Chu, S. (1986). Observation of a single-beam gradient force optical trap for dielectric particles, *Opt. Lett.* 11(5): 288–290.

Box, G. E. P. & Lucas, H. L. (1959). Design of experiments in non-linear situations, *Biometrika* 46: 77–90.

Dame, R. T., Noom, M. C. & Wuite, G. J. L. (2006). Bacterial chromatin organization by H-NS protein unravelled using dual DNA manipulation, *Nature* 444(16): 387–390.

Emiliani, V., Sanvitto, D., Zahid, M., Gerbal, F. & Coppey-Moisan, M. (2004). Multi force optical tweezers to generate gradients of forces, *Opt. Express* 12(17): 3906–3910.

Gong, Z., Chen, H.-T., Xu, S.-H., Li, Y.-M. & Lou, L.-R. (2006). Monte-carlo simulation of optical trap stiffness measurement, *Opt. Commun.* 263: 229–234.

Horst, A. v. d. & Forde, N. R. (2008). Calibration of dynamic holographic optical tweezers for force measurements on biomaterials, *Opt. Express* 16(25): 20987–21003.

Kozawa, Y. & Sato, S. (2010). Optical trapping of micrometer-sized dielectric particles by cylindrical vector beams, *Opt. Express* 18(10): 10828–10833.

Li, T., Kheifets, S., Medellin, D. & Raizen, M. G. (2010). Measurement of the instantaneous velocity of a Brownian particle, *Science* 328(5986): 1673–1675.

Liao, G.-B., Bareil, P. B., Sheng, Y. & Chiou, A. (2008). One-dimensional jumping optical tweezers for optical stretching of bi-concave human red blood cells, *Opt. Express* 16(3): 1996–2004.

McCann, L. I., Dykman, M. & Golding, B. (1999). Thermally activated transitions in a bistable three-dimensional optical trap, *Nature* 402: 785–787.

Mio, C., Gong, T., Terray, A. & Marr, D. W. M. (2000). Design of a scanning laser optical trap for multiparticle manipulation, *Rev. Sci. Instrum.* 71(5): 2196–2200.

Ou-Yang, H. D. (1999). Design and applications of oscillating optical tweezers for direct measurements of colloidal forces, *Colloid-Polymer Interactions: From Fundamentals to Practice*, John Wiley and Sons, New York.

Pesce, G., Luca, A. C. D., Rusciano, G., Netti, P. A., Fusco, S. & Sasso, A. (2009). Microrhoelogy of complex fluids using optical tweezers: a comparison with macrorhoelogical measurements, *J. Opt. A: Pure Appl. Opt.* 11: 034016.

Ren, Y.-X., Li, M., Huang, K., Wu, J.-G., Gao, H.-F., Wang, Z.-Q. & Li, Y.-M. (2010). Experimental generation of Laguerre-Gaussian beam using digital micromirror device, *Appl. Opt.* 49(10): 1838–1844.

Ren, Y.-X., Wu, J.-G., Chen, M., Li, H. & Li, Y.-M. (2010). Stability of novel time-sharing dual optical tweezers using a rotating tilt glass plate, *Chinese Physics Letters* 27(2): 028703.

Ren, Y.-X., Wu, J.-G., Zhong, M.-C. & Li, Y.-M. (2010). Monte carlo simulation of effective stiffness of time-sharing optical tweezers, *Chinese Optics Letters* 8(2): 170–172.

Ren, Y.-X., Wu, J.-G., Zhou, X.-W., Fu, S.-J., Sun, Q., Wang, Z.-Q. & Li, Y.-M. (2010). Experimental generation of Laguerre-Gaussian beam using angular diffraction of binary phase plate, *Acta Physica Sinica(In Chinese)* 59(6): 3930–3935.

Sasaki, K., Koshioka, M., Misawa, H., Kitamura, N. & Masuhara, H. (1991). Pattern formation and flow control of fine particles by laser-scanning micromanipulation, *Opt. Lett.* 16(9): 1463–1465.

Seol, Y., Visscher, K. & Walton, D. B. (2004). Suppression of noise in a noisy optical trap, *Physical Review Letters* 93(16): 160602.

Wu, J.-G., Ren, Y.-X., Wang, Z.-Q., Zhou, C. & Li, Y.-M. (2009). Time-sharing multiple optical tweezers using rotating glass plate, *Chinese J. Lasers (In Chinese)* 36(10): 2751–2756.

Zhang, Y., Smith, C. L., Saha, A., Grill, S. W., Mihardja, S., Smith, S. B., Cairns, B. R., Peterson, C. L. & Bustamante, C. (2006). DNA translocation and loop formation mechanism of chromatin remodeling by SWI/SNF and RSC, *Molecular Cell* 24(4): 559–568.

Zhou, M., Yang, H., Di, J. & Zhao, E. (2008). Manipulation on human red blood cells with femtosecond optical tweezers, *Chin. Opt. Lett.* 6(12): 919–921.

Applications of Monte Carlo Method in Science and Engineering
Edited by Prof. Shaul Mordechai

ISBN 978-953-307-691-1
Hard cover, 950 pages
Publisher InTech
Published online 28, February, 2011
Published in print edition February, 2011

In this book, Applications of Monte Carlo Method in Science and Engineering, we further expose the broad range of applications of Monte Carlo simulation in the fields of Quantum Physics, Statistical Physics, Reliability, Medical Physics, Polycrystalline Materials, Ising Model, Chemistry, Agriculture, Food Processing, X-ray Imaging, Electron Dynamics in Doped Semiconductors, Metallurgy, Remote Sensing and much more diverse topics. The book chapters included in this volume clearly reflect the current scientific importance of Monte Carlo techniques in various fields of research.

InTech Europe
University Campus STeP Ri
Slavka Krautzeka 83/A
51000 Rijeka, Croatia
Phone: +385 (51) 770 447
Fax: +385 (51) 686 166
www.intechopen.com

InTech China
Unit 405, Office Block, Hotel Equatorial Shanghai
No.65, Yan An Road (West), Shanghai, 200040, China
中国上海市延安西路65号上海国际贵都大饭店办公楼405单元
Phone: +86-21-62489820
Fax: +86-21-62489821

IntechOpen